Band offsets and lattice-mismatch effects in strained-layer CdTe/ZnTe superlattices

H. Mathieu, J. Allegre, A. Chatt, and P. Lefebvre
Groupe d'Etudes des Semiconducteurs, Université des Sciences et Techniques du Languedoc, 34060 Montpellier Cédex, France

J. P. Faurie
Department of Physics, University of Illinois, Chicago, Illinois 60680
(Received 17 February 1988)

We present a detailed investigation of the combined effects of band offsets and lattice mismatch on the subband structure of strained-layer CdTe/ZnTe superlattices. It is shown that, depending on the layer thicknesses, the superlattice may either have a type-I configuration, where electron and hole are mostly localized within CdTe layers, or a type-II configuration. Moreover, the hole ground state may either be the heavy-hole subband or the light-hole one. The results are compared with photoluminescence data and the value $\Delta E_v = 60 \pm 20$ meV is obtained for the zero-strain valence-band offset.

I. INTRODUCTION

Strained-layer superlattices (SLS's) receive great attention today, due to their intrinsic interest and possible applications to electronic devices. Strain effects in superlattices may have different origins: First, a lattice-matched multilayer structure may be submitted to an external stress which may either be hydrostatic or uniaxial. The elastic strain gives rise to a number of interesting properties like shift and mixing of the energy states.[1-9] Second, the multilayer structure may be grown lattice mismatched with the substrate. In that case, depending on the layer thickness the mismatch strain is accommodated coherently or by misfit dislocations.[10-12] Third, the multilayers may be lattice mismatched between them.[13-16] In this last case the strained-layer superlattice may either be free standing or in strain equilibrium with a buffer layer.[17] In the first case the strain energy is stored solely in the superlattice, in the second case the strain is distributed between both sets of layers, superlattice and buffer. Now, in all cases, a strained layer is sensitive not only to atomic misfit but also to layer thickness. As a critical thickness is exceeded, the misfit dislocation density at the layer interface increases sharply, relieving elastic strain. Below the critical thickness the accommodation of the lattice mismatch by elastic strain induces change in electronic properties which may quantitatively be comparable to quantum-size effect.

In this paper, we present a detailed investigation of the combined effects of band offsets and lattice mismatch on strained-layer CdTe/ZnTe superlattices. The first effect is an intrinsic one, but the strain effect, resulting from the lattice mismatch, is a function of the layer thicknesses. It is shown that depending on the relative values of the two effects, the CdTe/ZnTe SLS's may either be type I for the electron–heavy-hole system and type II for the electron–light-hole system, or type I for both systems, or type II for both systems. Moreover, depending on the layer thicknesses, the difference between the zero-strain valence-band offset and the strain-induced splitting of the valence bands may induce a reversal of the energy position of the heavy- and light-hole subbands. The hole ground state may either be the light- or heavy-hole subband. The results are compared with experimental data obtained on several CdTe/ZnTe SLS's grown by molecular-beam epitaxy (MBE) on (100)-oriented GaAs substrates. We deduce a zero-strain valence-band offset $\Delta E_v = 60$ meV in agreement with the common-anion rule.

II. THEORETICAL BACKGROUND

We calculate the superlattice band structure in the Kronig-Penney model, taking account of both the band offsets and the lattice-mismatch effect.

Let us first consider the zero-stress band offsets. They may be written as

$$\Delta E_c = E_{c_2} - E_{c_1} = K \, \Delta E_g \ , \tag{1a}$$

$$\Delta E_v = E_{v_2} - E_{v_1} = (K-1)\Delta E_g \ . \tag{1b}$$

Hereafter, and throughout the paper, the subindex 1 corresponds to CdTe and 2 to ZnTe. The low-temperature gap offset is taken as $\Delta E_g = E_{g_2} - E_{g_1} = 2391 - 1606 = 785$ meV. It is to be noted that, on account of the common anion rule,[18] K is expected to be close to 1.

Let us now consider the lattice-mismatch effect. The lattice mismatch $\Delta a/a = 6.2\%$ between the two compounds gives rise to a biaxial strain which shifts the band extrema and splits the valence-band degeneracy. In all the zinc-blende-type crystals the heavy-hole band is pushed above the light-hole one for biaxial compression and below for biaxial dilatation. Hence concerning the CdTe/ZnTe superlattices the valence-band maximum is defined by the heavy-hole band in CdTe and by the light-hole band in ZnTe.

The strain effects are completely expressed in terms of the lattice mismatch, the elastic compliance constants,

and the deformation potentials of the Γ_6 conduction-band minimum and Γ_8 valence-band maximum of CdTe and ZnTe.

The elastic compliance constants are taken from McSkimin *et al.*[19] for CdTe and from Berlincourt *et al.*[20] for ZnTe. The values are given in Table I.

The in-plane lattice parameter $a_\perp$ is obtained by minimizing the deformation energy. A simple calculation gives

$$a_\perp = \frac{a_b L_b / S_b a_b^2 + N(a_1 L_1 / S_1 a_1^2 + a_2 L_2 / S_2 a_2^2)}{L_b / S_b a_b^2 + N(L_1 / S_1 a_1^2 + L_2 / S_2 a_2^2)} , \quad (2)$$

where $S_i = (S_{11} + S_{12})_i$ with $i=1$ for CdTe, $i=2$ for ZnTe, and $i=b$ for the buffer layer. L_b, L_1, and L_2 are, respectively, the buffer layer, the CdTe layer, and the ZnTe barrier thickness. N is the period number of the superlattice. It is to note that the superlattice may either be positively or negatively strained, depending on the buffer-layer type (CdTe, ZnTe, or CdZnTe alloy).

If the superlattice is free standing, the actual strain distribution and the in-plane lattice constant are independent of the buffer layer and $a_\perp$ is written as

$$a_\perp = \frac{a_1 L_1 / S_1 a_1^2 + a_2 L_2 / S_2 a_2^2}{L_1 / S_1 a_1^2 + L_2 / S_2 a_2^2} . \quad (3)$$

Note that on account of the very large differences between the elastic compliance constants and between the lattice parameters, it is not possible to simplify Eq. (3).

The epitaxial layers experience a tetragonal distortion resulting in a very simple form of the strain tensor. The biaxial in-plane strain has only diagonal components:

$$e_{xx_i} = e_{yy_i} = \frac{a_\perp - a_i}{a_i} , \quad (4a)$$

$$e_{zz_i} = -\frac{a_\perp - a_i}{a_i} (2C_{12}/C_{11})_i , \quad (4b)$$

where C_{ij} are the elastic stiffness constants.

The correspoding equivalent stress tensor experienced by each type of layer is diagonal with the components given by

$$X_{xx_i} = X_{yy_i} = X_i = \frac{a_\perp - a_i}{a_i} \frac{1}{(S_{11} + S_{12})_i} , \quad (5a)$$

$$X_{zz_i} = 0 . \quad (5b)$$

TABLE I. Elastic compliance constants and deformation potentials of CdTe and ZnTe used in the calculations.

Parameters	CdTe	ZnTe
S_{11} (10^{-6} bar^{-1})	4.25	2.40
S_{12}	−1.73	−0.873
S_{44}	5	3.21
a_c (eV)	−2.15	−3.5
a_v (eV)	1.18	1.8
b (eV)	−1.4	−0.92
d (eV)	−3.5	−3.3

Now, one can readily apply the phenomenological deformation-potential theory to calculate the strain effect on the conduction- and valence-band extrema. The energy shifts and splitting are written

$$E_{c_i} = 2a_{c_i}(S_{11} + 2S_{12})_i X_i , \quad (6a)$$

$$E_{\mathrm{hh}_i} = 2a_{v_i}(S_{11} + 2S_{12})_i X_i - b_i(S_{11} - S_{12})_i X_i , \quad (6b)$$

$$E_{\mathrm{lh}_i} = 2a_{v_i}(S_{11} + 2S_{12})_i X_i + b_i(S_{11} - S_{12})_i X_i , \quad (6c)$$

where a_{c_i} and a_{v_i} are the hydrostatic deformation potentials of the conduction and valence bands, respectively, and b_i are the shear deformation potentials of the valence bands.

Before we calculate the energy states, and on account of the very different values proposed in literature, let us first discuss the deformation-potential values used in the present calculation. The hydrostatic deformation potentials a_{c_i} and a_{v_i} are obtained in the following way: The experimental values of $(dE_g/dP)_i$ are taken from Babonas *et al.*[21] for CdTe and from Strossmer *et al.*[22] for ZnTe. We deduce the band-gap hydrostatic deformation potentials $a_1 = -3.3$ eV and $a_2 = -5.3$ eV. Then we use the calculated values of the ratio a_{c_i}/a_{v_i} given by Camphausen *et al.*[23] to obtain a_{c_i} and a_{v_i}; the values are given in Table I. Concerning the shear deformation potential b_1 of CdTe, we use the experimental data given by Thomas,[24] normalized with the value of dE_g/dP taken from Babonas *et al.* The shear deformation potential b_2 of ZnTe is obtained from the experimental data given by Kaplyanskii *et al.*,[25] normalized with the value of dE_g/dP taken from Strossmer *et al.* The values of b_1 and b_2 are given in Table I. In the same way we deduced the trigonal deformation potential d_i given in Table I.

The electron and hole potential wells result from both the band offsets and the lattice-mismatch effect. The strain splitting being comparable to the zero-strain valence-band offset, one may expect the hole level pattern to be completely reorganized by the strain field.

The potential wells are written

$$V_e = K\,\Delta E_g + \Delta V_e , \quad (7a)$$

$$V_{\mathrm{hh}} = (K-1)\Delta E_g + \Delta V_{\mathrm{hh}} , \quad (7b)$$

$$V_{\mathrm{lh}} = (K-1)\Delta E_g + \Delta V_{\mathrm{lh}} , \quad (7c)$$

with $\Delta V_e = E_{c2} - E_{c1}$, where E_{c_i} are the strain shifts of the conduction-band minima given by Eq. (6a). ΔV_e represents the strain contribution to the electron potential wells. ΔV_{hh} and ΔV_{lh} have the same meaning for the heavy and light holes, respectively.

Different configurations are expected depending on the relative magnitudes of the zero-strain valence-band offset (K parameter) and of the lattice-mismatch effect (X_i parameters). First of all, on account of the values of the parameters, let us note that V_e is always positive so that the CdTe layers correspond to quantum wells for the electrons. This is not so clear for the holes. As a matter of example, let us consider the free-standing case which is

likely to correspond to CdTe/ZnTe superlattices.[16] In that case the X_i parameter is only a function of the ratio N_1/N_2, where $N_{1,2}$ is the monolayer number of each compound. Figure 1 shows the K dependence of the depth $|V_j|$ (j=hh,lh) of the heavy- and light-hole potential wells, for three different values of the ratio N_1/N_2. Note that the CdTe (ZnTe) layers correspond to the hole quantum wells if V_j is negative (positive), as a consequence different situations are possible depending on K. For $K \lesssim 0.7$ ($\Delta E_v \lesssim -240$ meV), both V_{lh} and V_{hh} are negative, so the CdTe layers are quantum wells for both the light and heavy holes. In that case the superlattice has a type-I configuration for both the electron–light-hole and electron–heavy-hole systems [see inset (a) in Fig. 1]. In this range of the K values the slope of the curves are negative, an increase of K give rise to a decrease of $|V_{lh}|$ and $|V_{hh}|$, the depths of the light- and heavy-hole quantum wells decrease. For $0.7 \lesssim K \lesssim 1.13$ ($-240 \lesssim \Delta E_v \lesssim 100$ meV) V_{hh} remains negative but V_{lh} becomes positive. The CdTe layers are still quantum wells for the electrons and the heavy holes but act as barriers for the light holes: The superlattice has a type-I configuration for the electron–heavy-hole system and a type-II configuration for the electron–light-hole system. [See inset (b) in Fig. 1.] Now $|V_{lh}|$, which is then located in the ZnTe layers, increases with increasing K; on the contrary, $|V_{hh}|$, which remains in the CdTe layers, still decreases. For $K \gtrsim 1.13$ ($\Delta E_v \gtrsim 100$ meV), the CdTe layers are only quantum wells for the electrons, the ZnTe layers are quantum wells for both the light and heavy holes; the superlattice has a type-II configuration [see inset (c) in Fig. 1], and both $|V_{lh}|$ and $|V_{hh}|$ are located in the ZnTe layers and increase with K. In the limiting case corresponding to $K \cong 0.7$ ($k \cong 1.13$) and the light (heavy) holes are not confined throughout the superlattice. In short, if $K \lesssim 0.7$ or $K \gtrsim 1.13$, the lattice-mismatch strain does not modify the superlattice type which is then defined by the zero-strain band offsets.

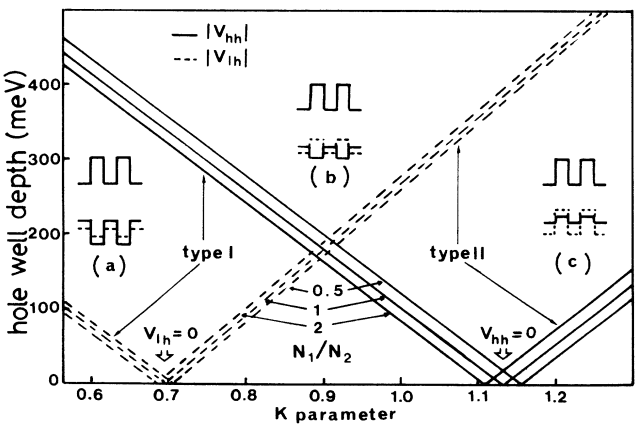

FIG. 1. K dependence of the depth of the light ($|V_{lh}|$) and heavy ($|V_{hh}|$) potential wells. A negative (positive) slope corresponds to a well localized in CdTe (ZnTe) and a barrier localized in ZnTe (CdTe).

However, in between these values, the strain splitting may be comparable to the zero-strain valence-band offset and the hole level pattern is completely reorganized by the strain field.

The different spatial localizations of the holes with varying K will have an important influence on the magnitude of the photoluminescence signal. If $K \lesssim 0.7$, one deals with the photoluminescence signal of a type-I system, this signal will be strong. Whereas if $k \gtrsim 1.13$ the photoluminescence signal is that of a type-II superlattice, which is expected to be weak. In between these values the luminescence signal is expected to be strong for the electron–heavy-hole transitions and weak for the electron–light-hole transitions.

In addition to the spatial localization, the energy-level distribution is a function of the relative magnitudes of the strain effect and zero-strain valence-band offset. The ground hole state may either be the heavy- or the light-hole state. We have calculated the superlattice band structure and the Brillouin-zone center energy gaps. The envelope-function approach, based on the effective-mass approximation, is easy to apply and gives a reasonable description of conduction and valence subbands provided the constituent materials are chemically similar, this is the case for the CdTe/ZnTe system. We have used the Kronig-Penney model with the standard boundary conditions, given by the continuity of both $F(z)$ and $1/m^*(z)$ $[\partial F(z)/\partial z]$, and taking into account the nonparabolicity effect on the effective masses. Let us label C_1, H_1, and L_1 the $k=0$ extrema of the electron, heavy-hole, and light-hole subbands, respectively. Figure 2 shows the K dependence of the C_1H_1 (solid lines) and C_1L_1 (dashed lines) band gaps at low temperature and for $N_1=N_2=5$, 10, and 15 monolayers. The figure is divided into three regions by two vertical dotted-dashed lines located at $K \cong 0.7$ and $K \cong 1.13$, respectively. In the first region ($K \lesssim 0.7$) the CdTe layers are quantum wells for the electrons and the heavy and light holes as discussed above, moreover it appears that the heavy-hole subband is always the ground state, so the fundamental gap of the SLS is $E_g = E(C_1H_1)$. Nevertheless, it is to note that this case is unlikely to exist in CdTe/ZnTe SLS because of the common anion rule which predicts a small value of the valence-band offset. The other regions are more likely to exist and different situations appear depending on the monolayer number. For the 5-5-SLS the heavy-hole subband remains the ground state of the valence band but the SLS configuration changes from type I to type II at $K \cong 1.13$. The case of the 10-10-SLS is a specific one, as the SLS configuration becomes type II, the light- and heavy-hole subbands become nearly degenerate at $K \cong 0$. Lastly, for the 15-15-SLS the light-hole subband becomes the ground hole state for $K \simeq 1.1$ ($\Delta E_v \simeq 80$ meV), and the SLS configuration becomes type II.

It seems, therefore, from these investigations that a careful study of the low-temperature photoluminescence and the identification of light- and heavy-hole transitions should provide useful information concerning the band offsets. Up to now the proposed values for the valence-band offset ΔE_v are the following: From indirect measurements based on the E_v position of CdTe and ZnTe

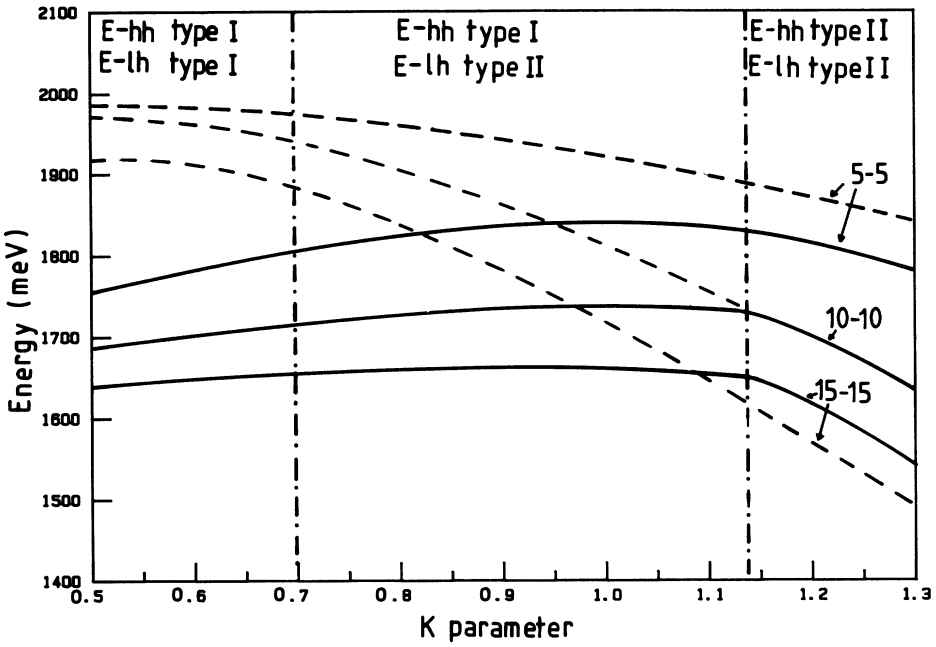

FIG. 2. K dependence of C_1H_1 (solid lines) and C_1L_1 (dashed lines) band gaps for 5-5, 10-10, and 15-15 superlattices.

relative to Ge, Katnani *et al.*[26] give $\Delta E_v = -100$ meV ($K=0.87$). From direct measurements, based on the core-level x-ray photoemission spectroscopy. Duc *et al.*[27] give the average value $\Delta E_v = 100 \pm 60$ meV ($1.05 < K < 1.20$). Lastly, Wei *et al.*[28] have proposed the calculated value $\Delta E_v = 130$ meV. Concerning the experimental value given in Ref. 27 it is worth noting that strain effects resulting from lattice mismatch between CdTe and ZnTe do not significantly affect the measurement. This results from the principle used for measuring ΔE_v: Two core levels E_{c1}, Cd $4d^5$ in CdTe and Zn $3d$ in ZnTe, are selected and their energy difference ΔE_{c1} across the interface is measured, then ΔE_v is deduced from this value and the energy difference $E_v - E_{c1}$ between the core level and the valence band for each isolated compound. In this way the lattice mismatch only affects the measurement of the core levels, which are not expected to be very sensitive to strain and anyway very much less sensitive than the valence-band maximum. So that the average value given in Ref. 27 corresponds to the parameter used in our calculation which has been defined as the zero-strain valence-band offset. Concerning the strain dependence of the core levels, one should note that the measurements of Duc *et al.*, which are made on very thin layers of ZnTe (CdTe) deposited on CdTe (ZnTe) substrate, have shown a noncommutativity in ΔE_{c1} between the two growth orders. This noncommutativity, which is 50 meV in the [111] heterojunction,[29] appears to be 170 meV in the [100] heterojunction,[29] but around an average value close to that of the [111] heterojunction. This may be related to the strain dependence of the core levels. In heterostructures such as CdTe/ZnTe the relative extent of the strain shift of these core levels may result from two reasons. First, the lattice mismatch is severe. Second, there exists in these II-VI compounds a substantial *p-d* hybridization between the cation *d* orbitals and the anion *p* orbitals, which in tetrahedral semiconductors have the same symmetry representation Γ_{15}. The strength of this hybridization results from the small value of the corresponding atomic-orbital energy difference which localizes the T_{15}^d core level inside the valence band and gives rise to 7.5% and 6.9% Γ_{15}^v character (valence-band maximum) for the Γ_{15}^d core level of ZnTe and CdTe, respectively.[28] Nevertheless the only *p-d* hybridization does not permit one to explain quantitatively the strong noncommutativity measured in [100] heterojunctions.

Now it should be noted that the range of the expected values of K ($1 \lesssim K \lesssim 1.2$) appears to select a very interesting region in Fig. 2: The properties of the SLS are very sensitive to the monolayer numbers; depending on N_1 and N_2 the SLS may be type I or II, and the hole ground state may be the light- or heavy-hole subband.

III. EXPERIMENTAL RESULTS

We wish to present results obtained on several CdTe/ZnTe superlattices grown by molecular-beam epitaxy on (100)-oriented GaAs substrates. Growth conditions have been described elsewhere,[15] the sample characteristics are given in the first part of Table II. The superlattices are grown on either CdTe, ZnTe, or $Cd_{0.5}Zn_{0.5}Te$ buffer layers, but the buffer-layer types do not seem to play an important role.[15,16] For a period number greater than about 30 the superlattice appears to be essentially

free standing,[30] so that the actual strain distribution and the in-plane lattice constant of the superlattice are independent of the buffer layer and substrate. In Table II we show the sample reference, the period number N, and the nominal thicknesses L_1^0 and L_2^0 of the CdTe and ZnTe layers determined through energy dispersive spectroscopy (EDS). Next the lattice parameters $a_\perp$, a_{z_1}, and a_{z_2} are calculated and the monolayer numbers N_1 and N_2, and the actual thicknesses L_1 and L_2, of each compound are deduced. L_1 and L_2 correspond, for the electron, to the well width and barrier thickness, respectively. The X_i parameters are the equivalent biaxial stress components, it is to note the very important values of this parameter in these SLS's. E_{c_i}, E_{hh_i}, and E_{lh_i} are the strain shifts of the band edges for each compound. Lastly ΔV_j ($j=e$, hh, and lh) are the strain contributions to the depth of the potential wells. ΔV_e positive and $\Delta V_{\mathrm{hh,lh}}$ negative increase (decrease) the depth of the corresponding potential well if located inside the CdTe (ZnTe) layers.

Now using the values of ΔV_j given in Table II and K as a fit parameter, we obtain the actual depth of the potential wells from Eqs. (7). Lastly we calculate the band gaps C_1H_1 and C_1L_1 in the framework of the Kronig-Penney model. Note that the strain-induced mixing between the spin-orbit split-off band $(\frac{1}{2},\frac{1}{2})$ and the valence band $(\frac{3}{2},\frac{1}{2})$ was neglected because of the large values of the spin-orbit splitting of CdTe ($\Delta_0=910$ meV) and ZnTe ($\Delta_0=920$ meV).[31] On the other hand the strain-induced mixing of the hole subbands was also ignored. Concerning the CdTe/ZnTe superlattices this is justified from symmetry considerations and localizations effects. The lattice-mismatch effect, which gives rise to an in-plane biaxial strain, has the same symmetry as the quantum-size effect. Consequently there is no strain coupling between the eigenstates of the wells. The zone-center energies of the various heavy- and light-hole subbands are strain shifted relative to each other without any coupling. A change in the valence-band structure may exist at $k_\parallel \neq 0$ due to variations of the $k_\parallel$ coupling between various heavy- and light-hole subbands as they are strain shifted relative to each other in energy. Now concerning this coupling, we believe it to be weak because the light and heavy holes are separated in the space (see Table IV). The heavy (light) holes are essentially localized inside the CdTe (ZnTe) layers.

Typical experimental results are given in Figs. 3 and 4. Figure 3 gives the photoluminescence spectra obtained at $T=2$ and 40 K on sample 6. Similar spectra are observed on samples 2, 6, 5, and 7. Clearly two structures appear which are labeled C_1H_1 and C_1L_1 in agreement with the theoretical interpretation. Figure 4 shows the photoluminescence spectra obtained on sample 1; similar spectra are obtained on sample 3. Several structures appear which are labeled C_1H_1, C_1L_1 for the high-energy structures and W_1, W_2 for the remaining ones. For all the samples the luminescence disappears at about 60 K.

Let us first discuss the C_1H_1 and C_1L_1 structures which exist in all the samples. For each sample the experimental values are compared to the calculated C_1H_1

TABLE II. Characteristics of the CdTe/ZnTe superlattices. X_i is positive for a dilatation and negative for a compression. $\Delta V_e<0$ corresponds to a decrease of the depth of the potential wells for the electrons if located inside the CdTe layers. $\Delta V_{\mathrm{hh}}<0$ ($\Delta V_{\mathrm{lh}}>0$) corresponds to an increase of the depth of the potential wells for the heavy (light) holes if located inside the CdTe (ZnTe) layers. The sample numbers 1, 2, 3, 4, 5, 6, 7 correspond, respectively, to the sample identification numbers 120-17, 122-18, 197-33, 198-39, 201-36, 206-40, and 207-41 as in Ref. 15.

Sample No.	N	L_1^0 (Å)	L_2^0 (Å)	L_1 (Å)	L_2 (Å)	a_{z_1} (Å)	a_{z_2} (Å)	$a_\perp$ (Å)	N_1	N_2	X_1 (kbar)	E_{c_1} (meV)	E_{hh_1} (meV)	E_{lh_1} (meV)	X_2 (kbar)	E_{c_2} (meV)	E_{hh_2} (meV)	E_{lh_2} (meV)	ΔV_e (meV)	ΔV_{hh} (meV)	ΔV_{lh} (meV)
1	400	23	17	23.7	17.7	6.79	5.90	6.25	7	6	−13.9	48.7	91	−143	17.5	−80.8	−10.5	94.8	−129	−101	237
2	250	30	36	30.8	35.7	6.84	5.95	6.21	9	12	−16.4	57.3	107	−168	13.3	−61.0	−7.96	71.6	−118	−115	240
3	200	28	21	27.2	20.7	6.79	5.90	6.24	8	7	−14.0	49.1	91.8	−145	17.3	−79.8	−10.4	93.7	−129	−102	238
4	200	27	30	27.3	29.7	6.83	5.94	6.22	8	10	−16.0	56.1	105	−165	13.9	−63.7	−8.30	74.9	−120	−113	240
5	200	21	30	20.6	29.8	6.87	5.97	6.19	6	10	−17.5	61.1	114	−180	11.3	−52.1	−6.80	61.2	−113	−121	241
6	200	26	33	27.4	32.7	6.85	5.95	6.21	8	11	−16.5	57.8	108	−170	13	−59.8	−7.80	70.2	−118	−116	240
7	200	34	36	34.2	35.6	6.83	5.93	6.22	10	12	−15.8	55.3	103	−163	14.2	−65.5	−8.54	76.9	−121	−112	240

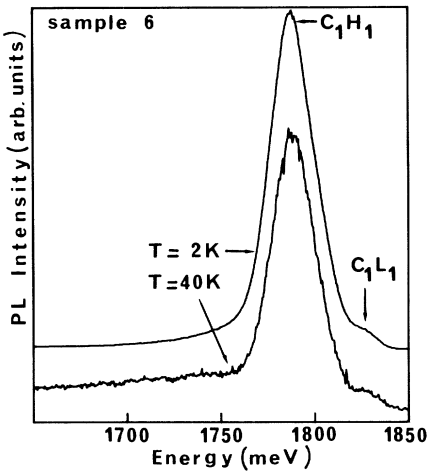

FIG. 3. Photoluminescence spectra of sample 6.

and C_1L_1 energy gaps as illustrated in Fig. 5. The experimental values appear as dashed horizontal lines and the calculated values as a function of the valence-band offset (K parameter) appear as solid lines. The vertical dotted-dashed lines have the same meaning as in Fig. 2. Clearly, for this sample the better fit is obtained with $K=1.05$ ($\Delta E_v=40$ meV) and shows that C_1H_1 corresponds to a type-I superlattice and C_1L_1 to a type-II superlattice. This is in agreement with the extent of the ratio of the luminescence intensities, $I(C_1H_1)/I(C_1L_1)$. All the experimental results and calculated values of the energy gaps are summarized in Table III. It is to note that the exciton binding energy which amounts to a few meV was neglected. Despite that, the agreement of the calculated values with the experimental data is quite satisfactory. For the valence-band offset we deduce the main value:

$$\Delta E_v=60\pm 20 \text{ meV} .$$

This value is in very good agreement with the corresponding one (100±60 meV) proposed by Duc *et al.*[27] from core-level x-ray photoemission spectroscopy.

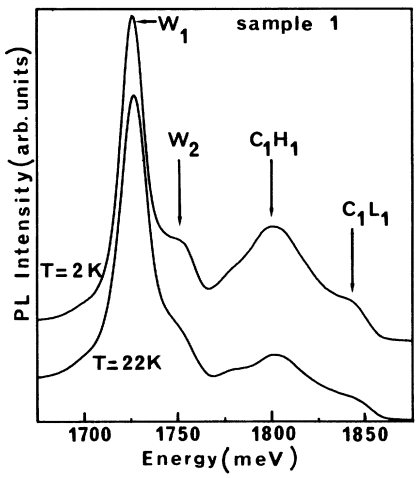

FIG. 4. Photoluminescence spectra of sample 1.

By using the new formalism of the Kronig-Penney model proposed by Hung-Sik Cho *et al.*,[32] we have calculated the width of the first electron and hole subbands ΔB_j and the probabilities to find the carriers inside the CdTe and ZnTe layers. The wave functions corresponding to the minimum energy of a given odd index subband ($n=1$) have even parity and can be written as (see Fig. 6)

$$\psi_i^{\min}(z)=A\cos[\alpha(z-L_i/2)] , \tag{8a}$$

$$\psi_j^{\min}(z)=B\cosh[\delta(z+L_j/2)] . \tag{8b}$$

(a) For the electrons (for which the CdTe layers act as quantum wells and ZnTe as barriers)

$$i=1,\quad j=2 ,$$

$$\alpha=\frac{1}{\hbar}(2m_{e_1}E_e^{\min})^{1/2} ,$$

$$\delta=\frac{1}{\hbar}[2m_{e_2}(V_e-E_e^{\min})]^{1/2} ,$$

where $E_e^{\min}$ is the minimum of the first subband for the electrons, and $m_{e_{1,2}}$ are the electron effective masses in CdTe and ZnTe, respectively.

(b) For the heavy holes

$$i=1,\quad j=2 ,$$

$$\alpha=\frac{1}{\hbar}(2m_{\mathrm{hh}_1}E_{\mathrm{hh}}^{\min})^{1/2} ,$$

$$\delta=\frac{1}{\hbar}[2m_{\mathrm{hh}_2}(V_{\mathrm{hh}}-E_{\mathrm{hh}}^{\min})]^{1/2} .$$

(c) For the light holes

$$i=2,\quad j=1 ,$$

$$\alpha=\frac{1}{\hbar}(2m_{\mathrm{lh}_2}E_{\mathrm{lh}}^{\min})^{1/2} ,$$

$$\delta=\frac{1}{\hbar}[2m_{\mathrm{lh}_1}(V_{\mathrm{lh}}-E_{\mathrm{lh}}^{\min})]^{1/2} .$$

TABLE III. Experimental and calculated values of the C_1H_1 and C_1L_1 energy gaps. The K value and the associated ΔE_v valence-band offset correspond to the better fit.

		Calculated values			
Sample	Experiment (eV)	C_1L_1 (eV)	C_1H_1 (eV)	K	ΔE_v (meV)
1	1.840	1.85		1.05	
	1.800		1.78		40
2	1.780	1.78		1.07	55
	1.747		1.74		
3	1.795	1.81		1.09	71
	1.768		1.76		
4	1.840	1.83		1.05	
	1.795		1.77		40
5	1.855	1.88		1.10	
	1.820		1.83		79
6	1.820	1.82		1.05	
	1.784		1.77		40
7	1.765	1.76		1.08	
	1.736		1.73		63

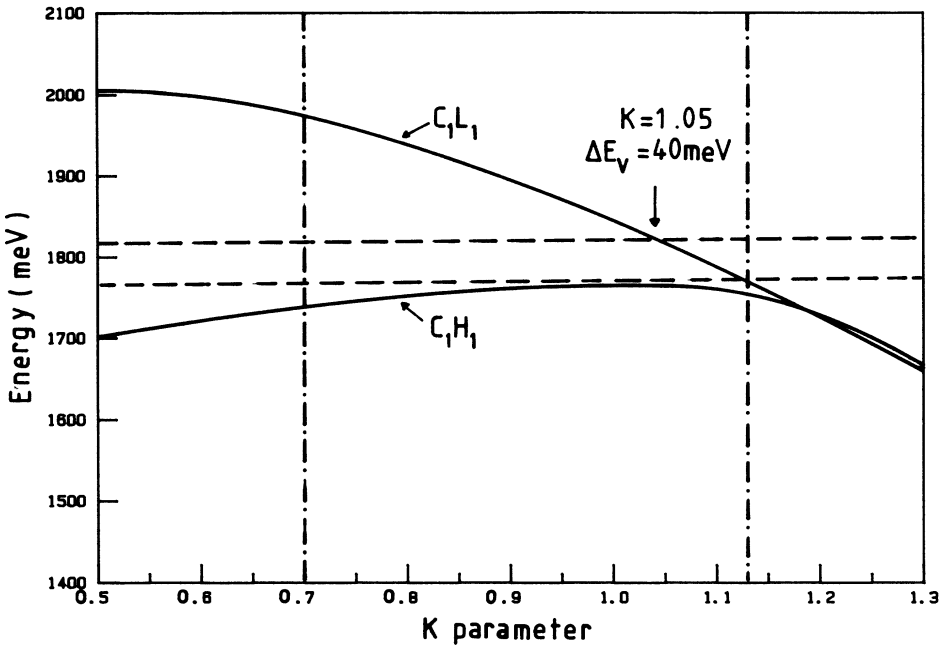

FIG. 5. Comparison of the measured and calculated values of the C_1H_1 and C_1L_1 transitions on sample 6.

The wave functions are obtained by using the minimum energy of the corresponding subband. The boundary condition $\psi_1^{\min}(0)=\psi_2^{\min}(0)$ is used thus eliminating a constant A or B, $B/A=\cos(\alpha L_i/2)/\cosh(\delta L_j/2)$. Now although these wave functions are not normalized, the probability to find the electron, or the hole, inside the CdTe or the ZnTe layers may be calculated. For each type of carrier these probabilities are given by

$$P_1=\frac{I_1}{I_1+I_2},\quad P_2=1-P_1\ ,$$

where

$$I_1=\int_0^{L_1}|\psi_1^{\min}(z)|^2dz$$

and

$$I_2=\int_{-L_2}^{0}|\psi_2^{\min}(z)|^2dz\ .$$

The calculated width of the electron, heavy-hole, and light-hole subbands, and the probabilities of finding each type of carrier inside the CdTe layers are given in Table

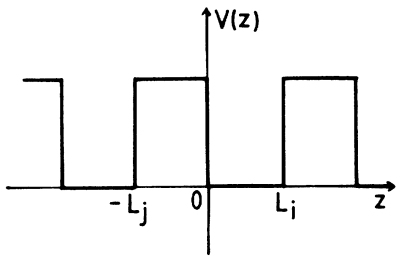

FIG. 6. Schematic view of the periodic square potential of the superlattice. L_i is the well width which corresponds to the CdTe layer thickness ($i=1$) for the electrons and the heavy holes and to the ZnTe layer thickness ($i=2$) for the light holes. L_j is the barrier thickness which corresponds to the ZnTe layer thickness ($j=2$) for the electrons and the heavy holes and to the CdTe layer thickness ($j=1$) for the light holes.

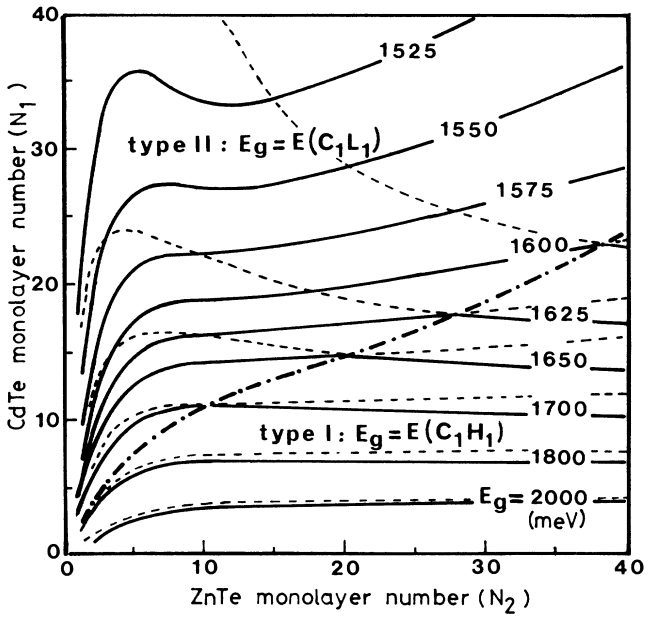

FIG. 7. Low-temperature CdTe-ZnTe superlattice band gap as a function of CdTe and ZnTe monolayer numbers per superlattice period. The dotted-dashed line corresponds to the C_1H_1-C_1L_1 crossing. Below (above) this line the band gap corresponds to the C_1H_1 (C_1L_1) transition and the superlattice has a type-I (II) configuration. Solid lines correspond to isoenergy gaps.

TABLE IV. Widths of the first subbands and probabilities of finding the carriers inside the CdTe layers.

Sample no.	ΔB_e (meV)	ΔB_{hh} (meV)	ΔB_{lh} (meV)	P^e CdTe (%)	P^{hh} CdTe (%)	P^{lh} CdTe (%)
1	58	15	89	81	75	41
2	3	2	13	90	83	15
3	29	14	49	86	70	33
4	9	3	27	87	82	21
5	15	11	37	80	60	19
6	6	2	21	87	83	18
7	2	2	9	92	83	14

IV. It clearly appears that the electrons and heavy-hole confinements in the CdTe layers are quite strong, with interwell coupling of the order of 10–20%. On the contrary the light holes are confined inside the ZnTe layers. These relatively strong confinements, associated with the thermalization effects, explain the important value of the ratio $I(C_1H_1)/I(C_1L_1)$. Moreover, this ratio is much more important in Fig. 3 compared to Fig. 4, this is in agreement with Table IV which shows a decrease of the carrier confinement in sample 1 compared to sample 6. Correspondingly the subband width increases as well as the three-dimensional (3D) character of the superlattice.

Let us now discuss the structures labeled W_1 and W_2 in Fig. 4. We believe these structures to result from finite interface roughness.[33] In the absence of roughness, the SLS energy states are organized in subbands and are extended throughout the whole structure. In the presence of disorder, resulting from interface roughness, the energy corresponding to extended states shrinks and localized levels appear with wave functions localized over a finite range of the SLS. Localized states corresponding to enlarged CdTe wells occur below each subband with electron and heavy-hole wave functions localized within the wells. We believe these energy-level features explain the luminescence structures labeled W_1 and W_2. A rough estimate of the energy states within a random CdTe well assumed isolated gives, for the electron, a localization energy of 24 and 46 meV below the bottom of the first conduction subband for a widening of two and three monolayers, respectively. The corresponding localization energies for the heavy holes are -0.5 and 2 meV. The resulting transition energies are 1755 and 1732 meV, respectively, which appear to be very close to the experimental values, 1750 and 1728 meV. A widening of only one monolayer has not been considered as localized enlarged wells because we believe these random enlarged wells to be sufficiently numerous to give rise to a broadening of the subband states in place of localized states. These subband tails lead to inhomogeneously broadened transitions which may be related to the spectral width (~ 30 meV) and probably to the low-energy shoulder of the C_1H_1 structure. On the other hand, note that a widening of three monolayers gives rise to localized states for both electrons and heavy holes but a widening of only two monolayers leads to localized states only for the electrons, the heavy-hole states appear as resonant ones. This is in agreement with the very strong intensity of the W_1 structure compared to the W_2 structure.

The appearance of these luminescence lines, associated to localized transitions, results from vertical transport of carriers. In other words, a part of the carriers photocreated in the superlattice move along the z axis and become trapped in the enlarged wells where they recombine. This vertical transport, has been unambiguously demonstrated by Chomette *et al.*[31] in $Ga_{1-x}Al_xAs$/GaAs superlattices. The authors have also shown that the efficiency of the vertical transport, which may be characterized by the ratio I_{W_i}/I_{SL}, where I_{W_i} and I_{SL} are the integrated intensities of the W_i and SL luminescences, increases with temperature. This agrees with the temperature dependence of this ratio which appears in Fig. 4, and supports our interpretation. In sample 1, as well as in sample 3, which present strong "extrinsic" low-energy structures, the vertical transport may be very important on account of the small value of the barrier thickness. The electron and the hole subband widths are important and the corresponding wave functions are extended throughout the superlattice (see Table IV). In the other samples studied here, the wave functions are much more localized and the vertical transport is expected to be weak, as a matter of fact no "extrinsic" transitions have clearly been observed.

In conclusions, we have reported theoretical investigation and experimental results on strained-layer CdTe/ZnTe superlattices. The combined effects of the band offsets and lattice mismatch give rise to a specific distribution of the hole subbands which is strongly influenced by the layer thicknesses. The fit of the experimental results leads to a small zero-strain valence-band offset $\Delta E_v \simeq 60$ meV in agreement with the common anion rule. Now, by using this parameter we have calculated the set of values of the CdTe and ZnTe monolayer numbers, N_1 and N_2, giving rise to a degenerate band gap for the superlattice, $E_g = E(C_1H_1) = E(C_1L_1)$. The result is illustrated by the dot-dashed line in Fig. 7. Below this line the ground state of the valence band is the heavy-hole subband, the band gap is $E_g = E(C_1H_1) < E(C_1L_1)$ and the superlattice has a type-I configuration. Above this line, the ground state of the valence band is the light-hole subband, the band gap is $E_g = E(C_1L_1) < E(C_1H_1)$ and the superlattice has a

type-II configuration. The isoenergy gaps are illustrated by solid lines. These lines correspond to C_1H_1 (C_1L_1) transitions below (above) the dot-dashed line. In the region where the C_1H_i ($i=1,2$) transition does not correspond to the smaller band gap, the isoenergy transitions are given as dotted lines. Note that a superlattice with a band gap inside the range $1.62 < E_g < 1.8$ eV may be obtained either with a type-I or a type-II configuration.

[1]C. Jagannath, E. S. Koteles, L. Johnson, Y. J. Chen, B. S. Elman, and J. Y. Chi, Phys. Rev. B **34**, 7027 (1986).

[2]P. Venkaterwaran, M. Chandrasekhar, H. R. Chandrasekhar, B. A. Vojak, F. A. Chambers, and J. M. Meese, Phys. Rev. B **33**, 8416 (1986).

[3]P. Lefebvre, B. Gil, J. Allegre, H. Mathieu, Y. Chen, and C. Raisin, Phys. Rev. B **35**, 1230 (1987).

[4]H. Mathieu, P. Lefebvre, J. Allegre, B. Gil, and A. Regreny, Phys. Rev. B **36**, 6581 (1987).

[5]P. Lefebvre, B. Gil, and H. Mathieu, Phys. Rev. B **35**, 5630 (1987).

[6]G. D. Sanders and Yia-Chung Chang, Phys. Rev. B **32**, 4282 (1985).

[7]G. Platero and M. Altarelli, in Proceedings of the Third International Conference on Modulated Semiconductor Structure (MSS-III), Montpellier, France, 1987 (unpublished).

[8]C. Mailhot and D. L. Smith, Phys. Rev. B **36**, 2942 (1987).

[9]L. C. Andreani, A. Pasquarello, and F. Bassani, Phys. Rev. B **36**, 5887 (1987).

[10]D. Gershoni, J. M. Vandenberg, R. A. Hamm, H. Temkin, and M. B. Panish, Phys. Rev. B **36**, 1320 (1987).

[11]M. C. Tamargo, R. Hull, L. H. Greene, J. R. Hayes, and A. Y. Cho, Appl. Phys. Lett. **46**, 569 (1985).

[12]Y. Matsui, M. Hayashi, M. Tokahashi, K. Kikuchi, and K. Yoshiba, J. Cryst. Growth **71**, 280 (1985).

[13]P. Voisin, M. Voos, J. Y. Marzin, M. C. Tamargo, R. E. Nahory, and A. Y. Cho, Appl. Phys. Lett. **48**, 1476 (1986).

[14]Y. Masakazu Kohayashi, M. Konagai, and M. Takahashi, J. Appl. Phys. **61**, 1015 (1987).

[15]G. Monfroy, S. Sivananthan, X. Chu, J. P. Faurie, R. D. Knox, and J. L. Standenmann, Appl. Phys. Lett. **49**, 152 (1987).

[16]R. H. Miles, G. Y. Wu, M. B. Johnson, T. C. McGill, J. P. Faurie, and S. Sivananthan, Appl. Phys. Lett. **48**, 1383 (1987).

[17]Y. Hefetz, D. Lee, A. V. Nurmikko, S. Sivananthan, Y. Chu, and J. P. Faurie, Phys. Rev. B **34**, 4423 (1987).

[18]W. Harrison, J. Vac. Sci. Technol. **14**, 1016 (1977).

[19]H. J. McSkimin ad D. G. Thomas, J. Appl. Phys. **33**, 56 (1962).

[20]D. A. Berlincourt, H. Jaffe, and L. R. Shiozawa, Phys. Rev. **129**, 1009 (1963).

[21]G. A. Babonas, R. A. Bendoryus, and A. Yu Shileika, Fiz. Tekh. Poluprovodn. **5**, 449 (1971) [Sov. Phys.—Semicond. **5**, 392 (1971)].

[22]K. Strossmer, S. Ves, Chul Koo Kim, and M. Cardona, Solid State Commun. **61**, 275 (1987).

[23]D. L. Camphausen, G. A. N. Connel, and W. Paul, Phys. Rev. Lett. **26**, 184 (1971).

[24]D. G. Thomas, J. Appl. Phys. Suppl. **32**, 2298 (1961).

[25]A. A. Kaplyanskii and L. G. Suslina, Fiz. Tverd. Tela (Leningrad) **7**, 2327 (1965) [Sov. Phys.—Solid State **7**, 1881 (1966)].

[26]A. D. Katnani and G. Margaritondo, Phys. Rev. B **28**, 1944 (1983).

[27]T. M. Duc, C. Hsu, and J. P. Faurie, Phys. Rev. Lett. **58**, 1127 (1987).

[28]S. H. Wei and A. Zunger, Phys. Rev. Lett. **59**, 144 (1987).

[29]T. M. Duc, C. Hsu, and J. P. Faurie, Phys. Rev. Lett. **59**, 947 (1987); C. Hsu and J. P. Faurie, J. Vac. Sci. Technol. B **6**, 773 (1988).

[30]G. Monfroy, M. Lange, X. Chu, and J. P. Faurie (unpublished).

[31]P. Lawaetz, Phys. Rev. B **4**, 3460 (1971).

[32]N. Hung-Sik Cho and Paul R. Prucnal, Phys. Rev. B **36**, 3237 (1987).

[33]A. Chomette, B. Deveaud, A. Regreny, and G. Bastard, Phys. Rev. Lett. **57**, 1464 (1986).